Materials Science and Engineering C 62 (2016) 860–869

Contents lists available at ScienceDirect

Materials Science and Engineering C

journal homepage: www.elsevier.com/locate/msec

High-permeability functionalized silicone magnetic microspheres with low autofluorescence for biomedical applications

Benjamin A. Evans *, Julia C. Ronecker, David T. Han, Daniel R. Glass, Tonya L. Train, Alison E. Deatsch

Elon University, 100 Campus Drive, Elon, NC 27244, USA

ARTICLE INFO

Article history:
Received 26 October 2015
Received in revised form 8 January 2016
Accepted 30 January 2016
Available online 13 February 2016

Keywords:
Magnetic microsphere
Magnetic nanoparticle
Silicone
Autofluorescence
Force spectroscopy
Drug delivery

ABSTRACT

Functionalized magnetic microspheres are widely used for cell separations, isolation of proteins and other biomolecules, in vitro diagnostics, tissue engineering, and microscale force spectroscopy. We present here the synthesis and characterization of a silicone magnetic microsphere which can be produced in diameters ranging from 0.5 to 50 μm via emulsion polymerization of a silicone ferrofluid precursor. This bottom-up approach to synthesis ensures a uniform magnetic concentration across all sizes, leading to significant advances in magnetic force generation. We demonstrate that in a size range of 5–20 μm, these spheres supply a full order of magnitude greater magnetic force than leading commercial products. In addition, the unique silicone matrix exhibits autofluorescence two orders of magnitude lower than polystyrene microspheres. Finally, we demonstrate the ability to chemically functionalize our silicone microspheres using a standard EDC reaction, and show that our folate-functionalized silicone microspheres specifically bind to targeted HeLa and Jurkat cells.

These spheres show tremendous potential for replacing magnetic polystyrene spheres in applications which require either large magnetic forces or minimal autofluorescence, since they represent order-of-magnitude improvements in each. In addition, the unique silicone matrix and proven biocompatibility suggest that they may be useful for encapsulation and targeted delivery of lipophilic pharmaceuticals.

1. Introduction

Micro-scale magnetic spheres have long been a valuable tool in biotechnology. The polymer matrix of the spheres generally allows for chemical functionalizations which enable specific, targeted binding of the product to selected materials. The magnetic component can then be called upon to provide a considerable force to the targeted materials across a large sample volume (mL) and without interacting substantially with the local environment. These properties have led to wide-scale adoption of magnetic microspheres for selective sequestration, separation, or concentration of proteins, peptides, nucleic acids, and cells [1–5]. Such techniques have led to the development of in vitro diagnostic (IVD) devices which utilize magnetic microspheres as a core technology to perform fluorescence immunoassays and other biosensing techniques for diagnostic effect [6–10].

Magnetic microspheres have also been adopted by the biophysics and biomedical engineering communities. Unlike more invasive force-clamp techniques such as optical trapping and AFM, magnetic microspheres do not induce local heating and may be activated and observed without direct contact. Thus, they comprise a leading modality for force spectroscopy, which enables experimenters to conduct non-invasive force and displacement measurements in various biologically-relevant environments, such as within the cell interior [11] or in the midst of polymer networks [12,13] or protein assemblies [14,15]. Single-molecule studies in particular have taken advantage of the non-contact force generated by magnetic microspheres to explore the topology of proteins or nucleic acids [16–19] or to control the translocation of biomolecules through a nanopore [19–21]. In addition, they have been used to probe mechanical properties and mechanotransduction in cells [22–25] and to influence cell differentiation in tissue engineering [26–28].

The majority of commercial magnetic microspheres consist of polystyrene microspheres [29] which are subsequently swollen in a solvent and saturation with a solution of iron oxide nanoparticles. A leading supplier of such microspheres is Invitrogen (Dynabeads), which produces small (1–4.5 μm) microspheres with well-controlled spherical morphology and narrow size distributions in a wide variety of surface functionalizations. These have been widely adopted for commercial use in IVD devices as well as in research and development within the biotech community. Their primary use is in separation and sequestration of proteins, peptides, and similar biomolecules or cells. A primary challenge in many of these applications is the presence of a significant autofluorescence signal which is native to the polystyrene matrix. This autofluorescence raises the noise floor in fluorescence-based assays, reducing their sensitivity.

* Corresponding author.
E-mail addresses: bevans7@elon.edu (B.A. Evans), julie.ronecker@gmail.com (J.C. Ronecker), dhan@elon.edu (D.T. Han), daniel.glass10@gmail.com (D.R. Glass), ttrain@elon.edu (T.L. Train), alison.e.deatsch.1@nd.edu (A.E. Deatsch).

http://dx.doi.org/10.1016/j.msec.2016.01.094
0928-4931/

Larger-diameter polystyrene magnetic microspheres, in the 5–20 μm range are commonly used in cell separations, tissue engineering, and force spectroscopy applications, in which the magnitude of the magnetic force is a primary consideration. The limiting factor in each of these applications is thus the magnetic content of the spheres, which is generally introduced by saturating polystyrene spheres with an iron oxide nanoparticle solution. Incomplete saturation of the microsphere bulk, however, results in a magnetization which does not scale linearly with volume, diminishing magnetic concentration in larger spheres.

We present here a bottom-up approach to microsphere fabrication which results in spheres with uniform magnetic content throughout their volume. We begin with a highly-permeable magnetic fluid consisting of magnetite nanoparticles coated in a silicone monolayer. The fluid is homogenous at scales below 100 nm, and no aggregation of constituent nanoparticles is evident. We form a colloidal suspension of the fluid in water with the aid of a surfactant, and crosslink the resulting emulsion to produce solid, spherical particles in diameters ranging from 0.5 to 50 μm. The result is a sphere with a constant magnetization per unit volume, which results in very large magnetic moments in larger spheres. We show that the resulting magnetic force is a full order of magnitude larger than that of leading polystyrene products of similar size. In addition, the silicone matrix native to our microspheres exhibits autofluorescence a full two orders of magnitude below that of leading polystyrene spheres.

Others have reported the synthesis of non-magnetic microspheres composed of silicone or silicone copolymers [30–36], but there have been remarkably few reports of magnetic silicone microspheres. The latter have been synthesized using methods such as ultrasonic spray pyrolysis [37] (<2 μm) and core-shell microfluidic extrusion [38] (>50 μm). However, most current work with magnetic microspheres occurs with commercially-available spheres in sizes ranging from 1 to 20 μm. Our work represents the first reported instance of a silicone magnetic microsphere spanning this critical size range, and the only reported instance of silicone magnetic microspheres between 2 and 50 μm.

Since silicone constitutes a new material for most existing magnetic microsphere applications, we show that the material is suitable for use in biotechnology. Silicone is widely recognized to be biocompatible, and does not interact chemically or osmotically in aqueous solutions. These same properties generally make the material difficult to functionalize. However, the presence of primary amines throughout the matrix of our formulation enables chemical functionalization of the microsphere surface. Specifically, in this work we demonstrate functionalization with folic acid via a standard EDC reaction, and show targeted specific binding of FA-labeled silicone magnetic microspheres to both HeLa and Jurkat cells, which over-express the folic acid receptor FRα. This same reaction may be used to functionalize the silicone spheres with a wide variety of ligands, making them immediately suitable for many existing applications.

These new silicone spheres represent order-of-magnitude improvements in autofluorescence signal and, in larger spheres (>5 μm), magnetic force application. The former can lead to dramatic improvements in the sensitivity of fluorescence-based IVDs, and the latter expands the scope of microscale mechanics and force spectroscopy. In addition, the soft lipophilic silicone matrix introduces new possibilities for encapsulation and delivery of poorly-soluble non-polar drug species. There have been many reports of microsphere formulations of hydrophilic matrices for drug delivery applications [39–41], yet relatively few reports of hydrophobic matrices and even fewer which include magnetic nanoparticles in hydrophobic matrices for stimulated release or targeting [42–46].

2. Materials and methods

2.1. Materials

Iron II chloride tetrahydrate ($FeCl_2 + 4H_2O$), iron III chloride ($FeCl_3$), ammonium hydroxide (28% NH_4OH), chloroform, methanol, cetyl trimethylammonium bromide (CTAB), hydrogen peroxide (30%), and formaldehyde (37%) were purchased from Fisher Scientific and used as received. Polyaminopropylmethylsiloxane-co-polydimethylsiloxane was purchased from Gelest (item #AMS-162). Alexa Fluor 488® Carboxylic Acid, Succinimidyl Ester, folic acid, and 1-ethyl-3-(3-dimethylaminopropyl)carbodiimide (EDC), as well as buffers MOPS (3-[N-Morpholino] Propane Sulfonic Acid, 0.1 M, pH 4–5), MES (2-[N-Morpholino] ethane-sulfonic acid, 0.1 M, pH 12), and PBS tablets were purchased from Sigma Aldrich and used as received. A BD Pharmingen™ FITC-conjugated Annexin V apoptosis detection kit was purchased from BD Biosciences and bovine serum albumin (BSA) was purchased from Santa Cruz Biotechnology.

2.2. Preparation of PDMS-coated magnetite nanoparticles

PDMS-coated magnetite nanoparticles were synthesized by previously reported methods [47], beginning with the formation of magnetite nanoparticles by the coprecipitation of iron salts [48]. Typically, iron II chloride tetrahydrate (7.4 g) and iron III chloride (12 g) were each dissolved into 150 mL of deionized water and then mixed together. After a few minutes, 80 mL concentrated ammonium hydroxide was added under vigorous stirring, and the mixture was allowed to continue to stir for 10 min. Next, polyaminopropylmethylsiloxane-co-polydimethylsiloxane (20 g) was added to the mixture which was stirred overnight, during which time the majority of the nanoparticles transferred to the polymer phase.

The resulting polymer complex was rinsed extensively with water and then with methanol to remove excess nanoparticles, salts, and unbound polymer. The rinsed material was suspended in chloroform and ultrasonicated in a bath for 30 min. This resulted in a silicone-based ferrofluid, termed '*FFPDMS*,' which remains diluted in chloroform for storage.

2.3. Magnetic characterization of precursor fluid

Magnetic nanoparticle concentration (wt.%) was determined by measuring the magnetic susceptibility of the FFPDMS precursor fluid with an MK1 magnetic susceptibility balance (Sherwood Scientific) and comparing with susceptibility measurements of uncoated dry magnetite nanoparticles. The FFPDMS solution was first diluted ~100× in chloroform to bring the magnetization down to a range accessible to the balance.

2.4. Fabrication of magnetic microspheres

Magnetic microspheres of varying diameter (1–100 μm) were fabricated by creating an emulsion of FFPDMS-chloroform solution in water. The concentration of the solution was first adjusted by evaporating or adding chloroform (to between 2:1 and 12:1 Chl:FFPDMS) and an aliquot of 25 μL of the resulting mixture was added to 20 mL of 0.5% CTAB solution warmed to 60 °C. The solution was immediately stirred on a vortex mixer at highest power for 10 s. After resting for 5 min, 600 μL of 37% formaldehyde was added to induce crosslinking. The resulting spheres were stored in a 0.5% CTAB solution and rinsed in deionized water prior to use.

2.5. Magnetic force measurements

To measure magnetic forces, microspheres were suspended in a viscous fluid and located a fixed distance (1.2 cm) from the face on the axis of a 1-cm cubic neodymium iron boride magnet. Spheres moved at constant velocity toward the magnet, and the resulting motion was recorded via video microscopy at 60× on a Nikon Eclipse Ti-S optical microscope. Magnetic forces were taken to be equal to viscous drag forces in this low-Reynolds system (Re ~ 10^5), which were calculated using Stoke's Law, wherein $F_{drag} = 6\pi * viscosity * radius * velocity$.

Microsphere velocities and radii were measured with video tracking software Spot Tracker (CISMM, http://cismm.cs.unc.edu) or by tracing in *ImageJ* (NIH, http://imagej.nih.gov), and all solution viscosities were measured with an AR-G2 rheometer (TA Instruments). Smaller FFPMDS microspheres, Dynabeads MyOnes and M-280s were suspended in a 0.5% CTAB/H2O solution, Spherotech microspheres were suspended in deionized water, and larger FFPDMS microspheres and Dynabeads M-450s were suspended in glycerine.

2.6. Characterization of autofluorescence

FFPDMS microspheres, Dynabeads M-450 (tosylactivated) microspheres, M-280 (tosylactivated) and MyOne (carboxylic acid) microspheres were each suspended in deionized water and imaged separately in a Nikon Eclipse Ti-S. Images were taken with a 60× objective in both brightfield and fluorescence. Excitation intensity was maximized and exposure times were varied from 1000 to 3000 ms. Images were analyzed with *ImageJ*. The fluorescence intensity of each particle was taken to be the average greyscale value within a circle centered on the particle, the diameter of which extended to the full width at half max (FWHM) of the greyscale value in a profile plot. Since brighter particles saturated the camera at the longer exposures necessary to image FFDPMS, exposure times were reduced accordingly and greyscale values for all measurements were normalized to 3000 ms. In addition, several representative images were taken with both Dynabeads and FFPDMS spheres in the same solution.

2.7. Chemical functionalization of microspheres

The microspheres were functionalized concurrently with both a fluorophore (Alexa Fluor 488®) and folic acid via an EDC reaction. The fluorophore was diluted 1:1000 in 5 mM DMSO, and 100 μL of the dilution was added to a solution of 10 mg EDC dissolved in 300 μL of 0.1 M MES. Similarly, 2.75 mg of folic acid was added to a solution of 5 mg EDC dissolved in 300 μL of 0.1 M MES. Microspheres (~0.5 mg) were rinsed (3× with ethanol, 3× with MOPS) and then suspended in 1 mL of 0.1 M MOPS. All three solutions were mixed vigorously and then rotated overnight while protected from light. The fluorophore and folic acid solutions were combined and added to 300 μL of the microsphere solution (to maintain a MES:MOPS ratio of 2:1), mixed vigorously, and rotated overnight. Finally, microspheres were washed 10× with PBS, suspended in 0.5 mL of PBS and stored at room temperature for up to one week. FTIR spectroscopy (Nicolet Magna 560 FT-IR) was used to verify that these spheres (FA+) were functionalized with folic acid.

To serve as a control for subsequent studies, a second solution of microspheres (FA−) was prepared identically except for the omission of the EDC linker in the initial folic-acid/MES solution.

2.8. HeLa and Jurkat T cell culture

The human cervical cancer cell line, HeLa, was maintained in DMEM/F12 with L-glutamine and HEPES buffer supplemented with 10% fetal bovine serum and 100 U/mL penicillin–streptomycin and amphotericin B (Invitrogen). The Jurkat human T lymphocytic leukemia cell line was maintained in RPMI media with 10% fetal bovine serum and 100 U/mL penicillin. Cells were grown at 37.0 °C and 5.0% CO_2.

2.9. Specific binding to HeLa cells via fluorescence microscopy

Cells were plated in 10 wells of a 96-well plate at a density of 12,000 cells per well (36,000 cells/cm^2) two days prior to the experiment and maintained in the DMEM/F12 media as described previously. Individual wells were dosed with either Alexa Fluor-488® conjugated FA+ spheres or FA− control spheres at a concentration of 20 μg/mL. The particles were allowed to incubate in culture for 30 min. After incubation, the cells were washed twice with DMEM/F12 and replaced with fresh media before imaging.

Cells were imaged using a Nikon Eclipse TE 2000-E inverted optical microscope (Nikon, Tokyo, Japan) with a 40X 0.75NA air objective. Fluorescence images were taken using a Photometrics Cascade II 512 electron multiplying CCD digital camera (Roper Scientific, Inc., Tuscon, AZ). The camera and filters were controlled using *μ-Manager* (http://valelab.ucsf.edu/~MM/MMwiki/). The samples were imaged in both bright field and fluorescence, and *ImageJ* was used to quantify the fraction of cell surface covered in bound microspheres.

2.10. Specific binding to Jurkat cells via flow cytometry

Fluorescent FA+ microspheres and fluorescent FA− controls (20 μg/mL) were each incubated for 30 min with suspended Jurkat T cells and rinsed and resuspended in PBS prior to analysis. Flow cytometry studies were completed with a Beckman-Coulter (Dako) CyAn ADP with an excitation of 488 nm and detection with a standard FITC detection filter. The software *Summit V4.3.01* provided instrumental control and data acquisition and analysis.

2.11. Microsphere effect on cell survival

To determine whether FFPDMS microspheres were toxic to human cells, Jurkat T-cells were incubated with 0–20 μg/mL microspheres for 24 h. FFPDMS were prepared to a concentration of 2 mg/mL in 20% bovine serum albumin in PBS. The average diameter of FFPDMS microspheres was 1.7 ± 1.3 μm, as measured by scanning electron microscopy. After incubation the cells were labeled with Annexin V-FITC and propidium iodide (PI) according to the manufacturer's procedure (BD Bioscience) and analyzed on a BD Accuri C6 flow cytometer. Cells were gated based on forward and side light scatter to exclude microspheres and debris from analysis. Annexin V-FITC and PI fluorescence were analyzed to determine viability.

3. Results and discussion

3.1. Morphology and size distribution

Magnetic microspheres produced by these methods are uniformly spherical, as evident in the SEM images shown in Fig. 1. Also clear in these images is the fact that the emulsion polymerization method produces populations of spheres with a wide distribution of diameters (Fig. 2). However, it is possible to control the average size of a population of microspheres produced by these methods by adjusting the viscosity of the precursor solution of FFPDMS-chloroform prior to the formation of the emulsion. This is done by adjusting the amount of chloroform in the solution by evaporation. In Fig. 2, we show that increasing the wt.% of FFPDMS in the FFPDMS/chloroform solution leads to a predictable increase in average sphere diameter. By this method, average sphere diameters are tunable across nearly three orders of magnitude (above ~100 μm, particles are no longer spherical; below 100 nm, we begin to be limited by the size of the constituent nanoparticles), allowing for the production of spheres to meet the needs of a wide variety of applications. For applications which require narrower size distributions, sphere solutions may be divided into monodisperse subpopulations by a variety of established techniques, including magnetophoresis [49,50], gravitational [51] or centrifugal [52] sedimentation, and a variety of continuous-flow microfluidic techniques [53] such as field-flow [54] or pinched flow fractionation [55].

3.2. Magnetic characterization

Previously published SQUID measurements [47] indicate that the magnetization of FFPDMS is linearly dependent on the percent weight

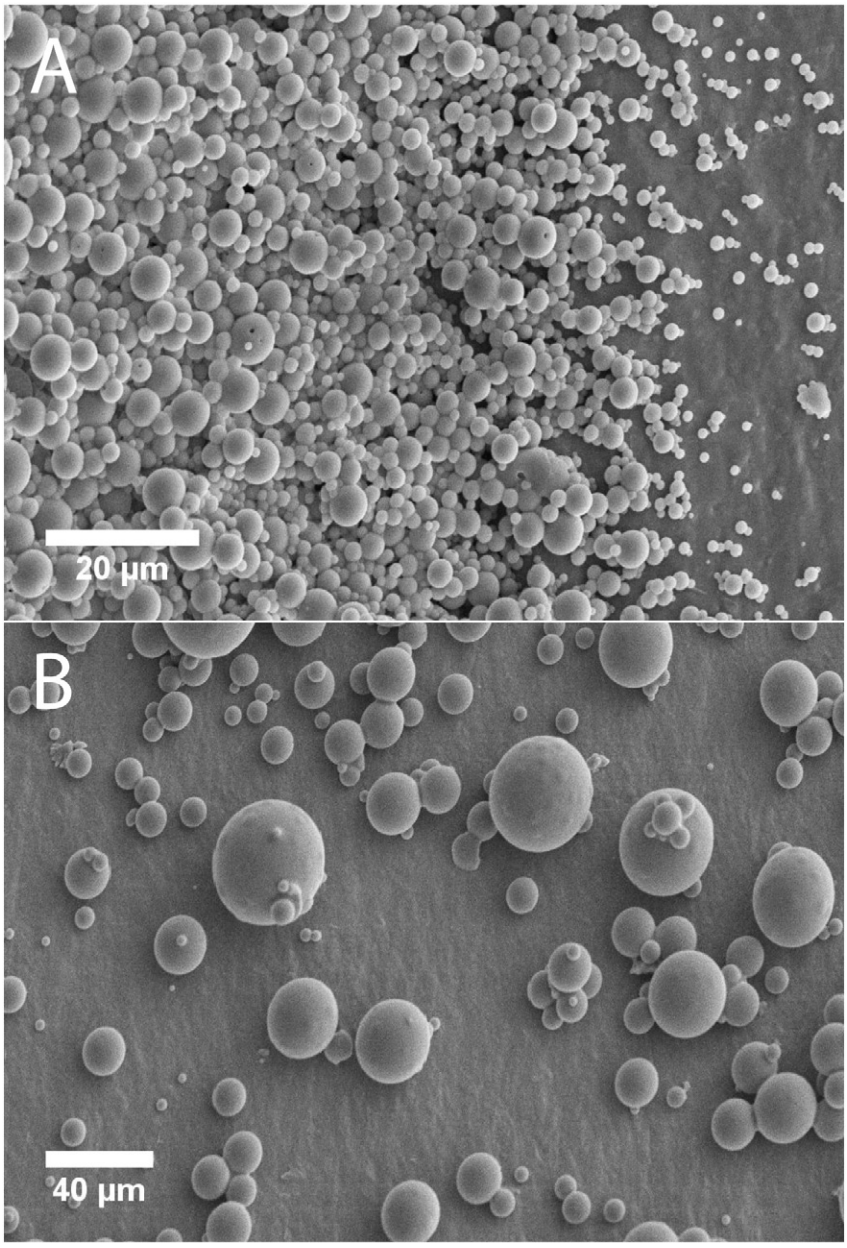

Fig. 1. Scanning electron micrographs of microspheres. Varying FFPDMS concentration by evaporating chloroform resulted in spherical particles of varying sizes. (A) 7.7% FFPDMS in chloroform formulation results in smaller spheres compared to (B) 20% FFPDMS in chloroform formulation.

loading of nanoparticles across a broad range of applied field (0–5 T) and nanoparticle loading (0–50 wt.% magnetite). This observation allows us to quickly quantify the magnetic content of the formulations of FFPDMS simply by comparing magnetic susceptibility measurements of each formulation to measurements on a 100% magnetite-nanoparticle standard. Susceptibility measurements indicate a loading of 48 ± 2 wt.% magnetite nanoparticles in the FFPDMS precursor, resulting in a calculated saturation magnetization of 40.6 ± 1.0 kA/m at 5 T. The magnetization can be tuned smoothly downward by adding additional polyaminopropylmethylsiloxane-co-polydimethylsiloxane to the precursor prior to the formation of the colloid.

Since FFPDMS spheres of all sizes are manufactured from the same precursor material, the nanoparticle concentration (and therefore the magnetic susceptibility) is identical for all sizes. This is evident in Fig. 3, which shows that magnetic force scales linearly with microsphere volume. This feature results in extraordinarily large forces for larger spheres, and also allows the experimenter to accurately predict applied forces by measuring sphere diameter in situ.

3.3. Magnetic force measurements

In many magnetic-microsphere applications, magnetic pulling force is a critical consideration. In general, the magnetic force on a microsphere with a magnetic moment m is given by the derivative of its potential energy with respect to a small spatial displacement; i.e. in one dimension, $F = -dU/dx$ where the potential energy $U = -m(B)B$. For a sphere with a uniform distribution of magnetic material, the moment is proportional to the volume of the sphere, V, and the loading fraction of magnetic nanoparticles, f, and so $m(B) = fM(B)V$, wherein $M(B)$ is the magnetization of the nanoparticles per unit volume. Thus, differentiating the energy yields

$$F = Vf\left[M(B) + B\frac{dM(B)}{dB}\right]\nabla B.$$

The first term represents the minimization of energy when a magnetic moment moves to a region of increased magnetic field (i.e.

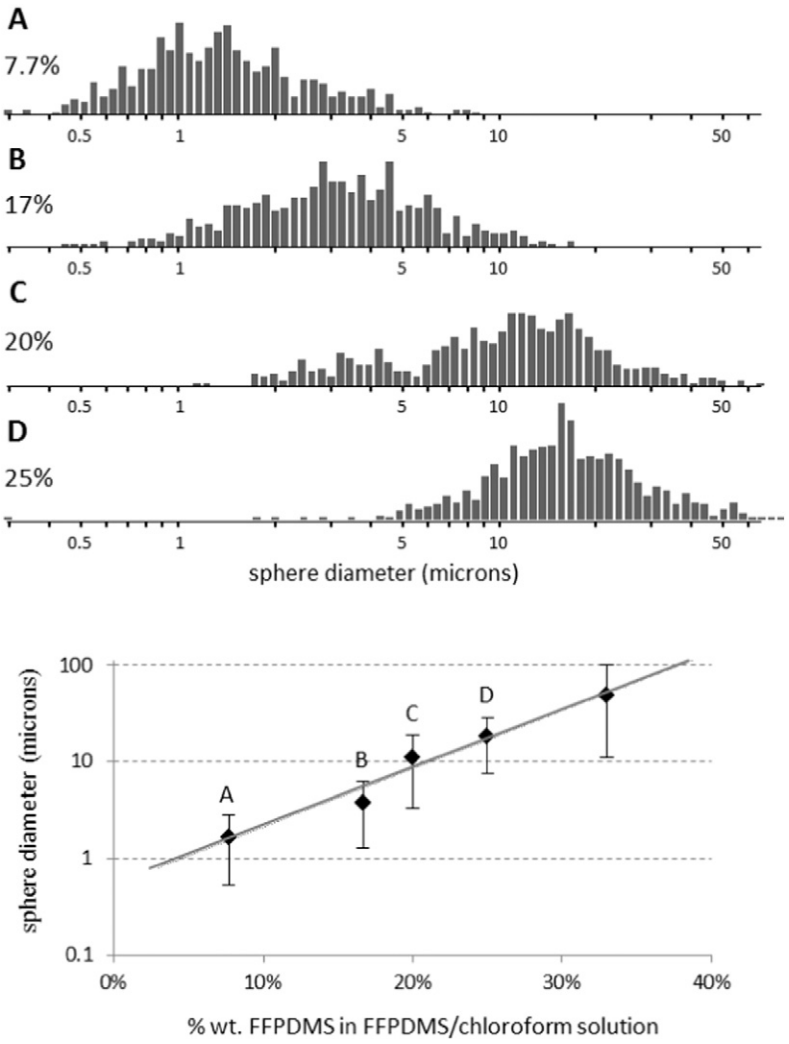

Fig. 2. Size distribution of FFPDMS spheres. Increasing the concentration of FFPDMS in the precursor fluid increases the average size of particles formed in the emulsion. Top: Four different formulations of microspheres produced of a precursor fluid containing (A) 7.7%, (B) 17%, (C) 20%, and (D) 25% FFPDMS (balance is chloroform). Larger spheres result from higher concentrations of FFPDMS in the chloroform mixture due to higher viscosity of the precursor fluid. Bottom: Average sphere diameter and standard deviation (bars) plotted as a function of wt.% FFPDMS in precursor, including the four formulations shown above. The trend can be used to predictably produce microspheres of a targeted size range between 1 and 100 μm.

increased B); the second represents the minimization of energy due to the increased magnetization of the material in a region of higher field (i.e. increased m). In the end, the magnetic force depends on three things: i) the choice of nanoparticle (contained in the term $M(B)$), ii) the magnetic field geometry (B,∇B), and iii) the total nanoparticle content of the microsphere (V,f). Nearly all commercially available magnetic microspheres contain magnetite nanoparticles, and so (i) is generally fixed, excepting small perturbations due to nanoparticle size and size distribution. The magnetic field geometry, by contrast, can vary dramatically from application to application – for example, magnetic separations such as magnetic-activated cell sorting (MACS) generally use permanent magnets positioned outside the sample volume, while experiments in membrane mechanics often rely on very closely-positioned electromagnetic poles with extremely large gradients [56]. The forces generated by identical beads in these disparate geometries can vary by orders of magnitude, and so here it is most useful to characterize magnetic forces in comparison to existing magnetic microsphere products. Force generation in any particular application can then be inferred, since regardless of field geometry, magnetic force will scale in proportion to the total nanoparticle content of the sphere.

In our measurements, we used a fixed magnetic field geometry produced by a single 1-cm^3 neodymium iron boride magnet positioned such that its north face was located 1.2 cm from the sample space, which was located on the magnetic axis. The magnet is fixed relative to the objective of the microscope, ensuring that the magnetic field geometry in the field of view is unaffected by translation of the sample stage or substitution of one sample for another. It is important to note that this magnetic field geometry is not designed to maximize magnetic force, but rather to provide a uniform magnetic force over the field of view while maintaining sphere velocities in a range appropriate for analysis via video microscopy. Thus the force magnitudes reported are not maximal – indeed, they are effectively arbitrary – but rather provide a meaningful comparison between products.

In Fig. 3, we show relative forces on two different formulations of our FFPDMS spheres (populations A and C from Fig. 2) alongside products from Dynabeads (Life Technologies) and Spherotech. It is clear that forces on our FFPDMS spheres are on par with Dynabeads, which is the industry leader in the 1–5 μm size range. More compelling, however, are the forces we measure on our larger (>5 μm) spheres, which are 1–2 orders of magnitude greater than forces on the leading commercial product in this size range. Larger spheres such as these may be used in cell separations or in mechanical studies of cells and tissues, in which large forces are required. By way of example, typical magnetic tweezer geometries can exert as much as 10 pN on Dynabeads MyOnes [57],

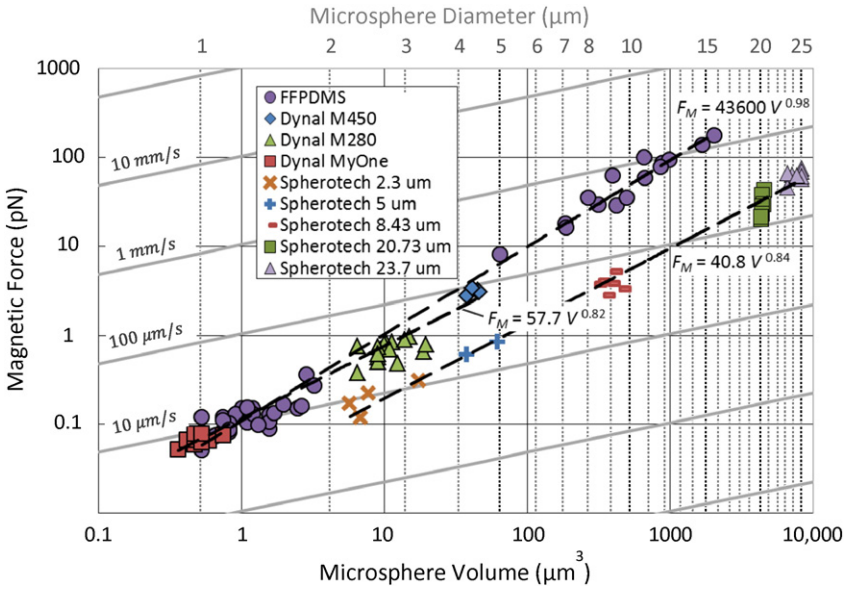

Fig. 3. Magnetic forces on microspheres. Spheres were suspended in a viscous fluid in a fixed magnetic field geometry, and magnetic forces were calculated from measurements of drift velocities of each particle. The magnetic field was not designed to optimize forces, but the relative values displayed here hold for any magnetic field geometry. Measurements indicate that magnetic nanoparticle concentration scales with volume in FFPDMS spheres, as expected. Constant-velocity lines in the plot indicate expected drift velocities for spheres in water ($\eta = 8.9 \times 10^{-4}$), which is particularly relevant to magnetic separation technologies.

yet a modestly-sized 10-μm FFPDMS sphere would experience 10 nN in the same tweezers — a force at the upper-limit of even AFM techniques [58].

An exponential fit to each product line (Fig. 3) indicates that magnetic nanoparticle loading is proportional to volume in the FFPDMS spheres.

3.4. Autofluorescence

In applications such as microbead-based immunofluorescence assays, any fluorescence signal native to the microbead (autofluorescence) constitutes experimental noise and reduces the sensitivity of the assay. Our autofluorescence experiments were conducted with both blue (488 nm) and green (568 nm) emission filters using maximum excitation intensity on a Nikon Eclipse Ti-S and exposure times of 1000–3000 ms. Longer exposure times were necessary to measure intensities of the FFDMS spheres, but other products required shorter exposure times to avoid saturating the 256 greyscale levels of the CCD. In the end, all fluorescence intensities were normalized to an exposure time of 3000 ms, and these data are shown in Fig. 4. In addition, we took several representative images of mixed populations of FFPDMS and polystyrene spheres (Fig. 4).

We find that our FFPDMS microspheres have an autofluorescence signal which is one to two orders of magnitude lower than polystyrene spheres and often indistinguishable or even below the background level (Fig. 4.) The absence of autofluorescence in the silicone matrix makes these FFPDMS spheres particularly well-suited for use in fluorescence-based assays.

3.5. Chemical functionalization

The utility of a magnetic microsphere is increased tremendously if the sphere can be functionalized with a variety of ligands for specific binding to a target. We show here that we are able to exploit the primary amines native to our FFPDMS to functionalize our spheres using a standard EDC reaction. In this particular instance, we bound both folic acid and a carboxy-terminated fluorophore to the spheres. Fig. 5 shows FTIR spectra of a) folic acid, b) unmodified FFPDMS microspheres, and c) FFPDMS microspheres functionalized with folic acid by the methods described in Section 2.7. Characteristic peaks from the folic acid at 2999 and 2915 cm^{-1} as well as 1500–1400 cm^{-1} are present in the functionalized spheres, yet the disappearance of the broad carboxylic acid peak at 3435 cm^{-1} and the carbonyl peak at 1659 cm^{-1} suggest that this group was modified in the reaction, as expected. Moreover, the addition of carboxy-terminated fluorophore to the reaction produced spheres which were clearly fluorescent, as evidenced by both fluorescence microscopy and the flow cytometry experiments described below. Taken together, this is clear evidence that primary amines are chemically available on the surface of the spheres. This same EDC reaction may be used to functionalize FFPDMS microspheres with any carboxylic acid, opening the doors to a broad range of chemical functionalization strategies.

3.6. Ligand-targeted specific binding to HeLa and Jurkat cells

The folic-acid functionalized spheres were used to demonstrate proof-of-concept ligand-targeted specific binding to both HeLa and Jurkat cell lines. The ligand-receptor interaction between folic acid and the glycosyl-phosphatidylinositol-anchored folate receptor FR-α has been previously investigated in cell uptake studies [59–63]. This interaction is particularly applicable because the FR-α is expressed on apical surfaces of epithelial cells and overexpressed on 40% of human cancers, including both HeLa and Jurkat [61]. In the following experiments, fluorescent folic-acid-conjugated spheres (FA+) were produced by the methods described in Section 2.7. A population of control spheres (FA−) was also manufactured using the exact same protocol with the exception of the EDC linker, which was omitted from the folic acid solution. This was done to control for the possibility of unbound, adsorbed folic acid on the sphere surface.

3.6.1. Plated HeLa cells

Fluorescent FA+ or FA− spheres were incubated with adherent HeLa cells and subsequently rinsed with a mild turbulent flow. Images were taken in both brightfield and fluorescence to determine the fraction of available cell surface covered with fluorescent spheres. Before rinsing, we show that cells incubated with both FA+ and FA− spheres show a similar fractional coverage (Fig. 6, left), which is to be expected due to gravitational settling. After rinsing, however, cells incubated with

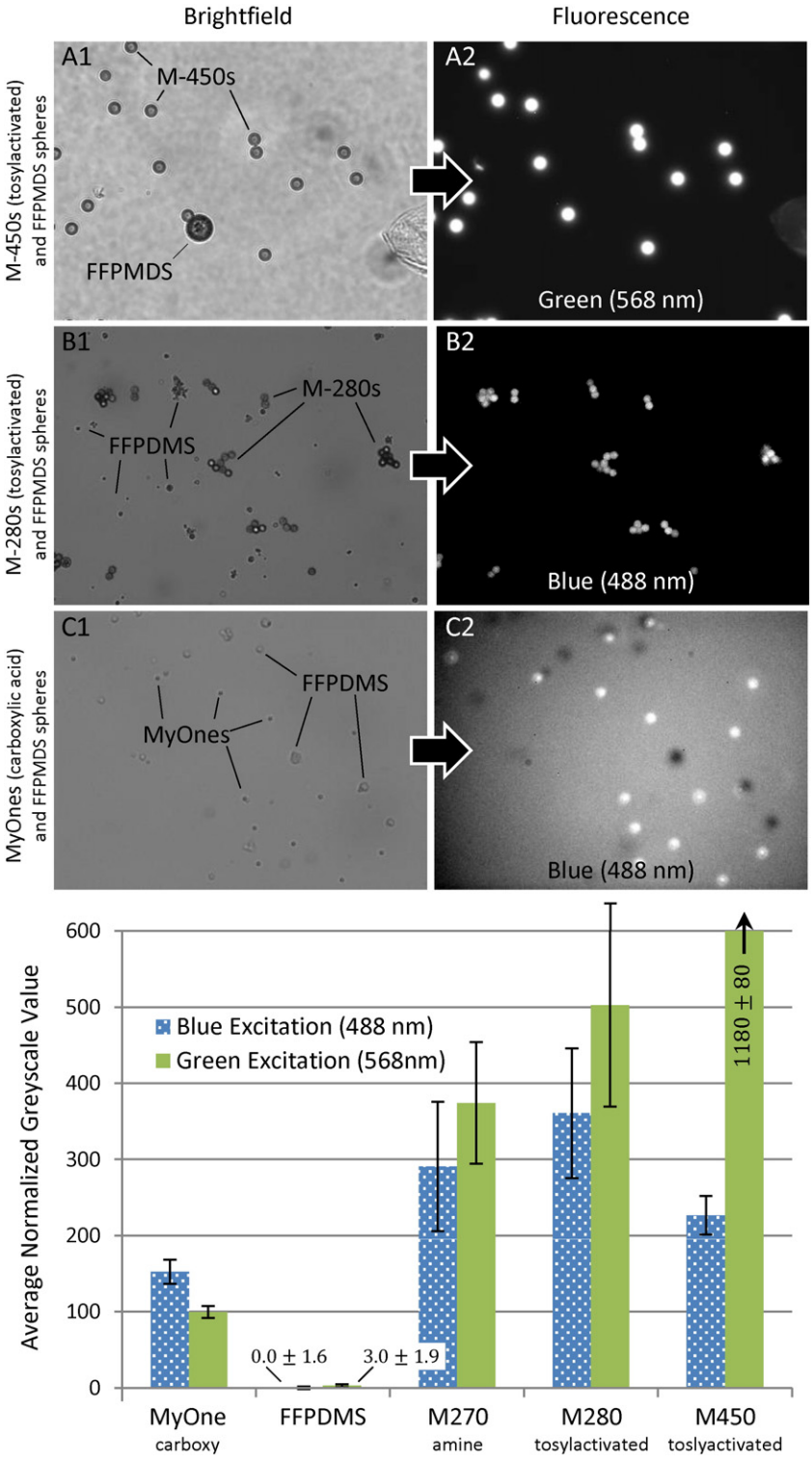

Fig. 4. Autofluorescence in magnetic microspheres. Top: Images at left (A1, B1, C1) show representative images of mixed populations of FFPDMS and polystyrene microspheres imaged in brightfield. The polystyrene beads in each image are distinguishable by their uniform diameters (A1: M-450s, 4.5 μm; B1: M-280s, 2.8 μm; C1: MyOnes, 1 μm), while FFPDMS spheres are polydisperse. Images at the right (A2, B2, C2) are fluorescence images of the same fields of view. Clearly evident is the relative absence of autofluorescence in the FFPDMS microspheres. Bottom: Measurements of average greyscale intensities of FFPDMS and polystyrene microspheres. Each sample in these measurements was imaged independently and greyscale values were normalized to a 3000 ms exposure time. Each measurement represents an average over at least ten particles.

FA + spheres showed a markedly increased coverage relative to the post-rinse FA − condition, which indicates that binding to the cell surface is mediated via the folic acid linker and is significantly stronger than non-specific adsorption. It is also notable that coverage in the FA + condition increased significantly during the rinsing step; this is due to increased incidence of contact during the turbulent rinse.

3.6.2. Suspended Jurkat cells

Fluorescent FA + or FA − spheres were incubated with suspended Jurkat cells as described in Section 2.10. Fluorescence intensity of unlabeled Jurkat cells, Jurkat cells incubated with FA − fluorescent spheres, and Jurkat cells incubated with FA + fluorescent spheres were measured via flow cytometry. Fig. 6 (right) shows a ten-fold increase in

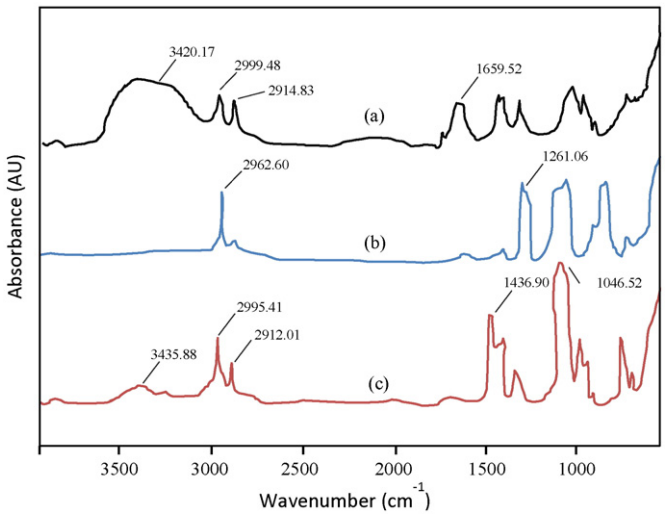

Fig. 5. FTIR indicates functionalization of microspheres with folic acid. Spectra of (a) folic acid (b) unmodified spheres and (c) functionalized spheres. Si-O stretches appear at 1022 cm^{-1} and 799 cm^{-1} (b) and a carboxylic acid peak is present at 3,420 cm^{-1} (a). Decreased 3420 cm^{-1} carboxylic acid absorbance peak suggests binding to amine terminal groups of magnetic microspheres, and shifted stretches in the 1309–1436 cm^{-1} range indicate chemical change.

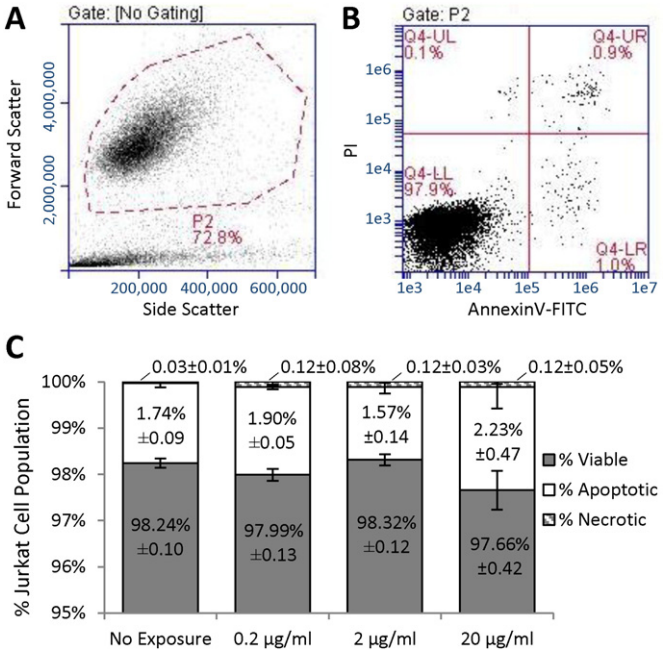

Fig. 7. Magnetic microsphere biocompatibility. Jurkat T-cells were incubated with varying concentrations of FFPDMS microspheres for 24 hours and analyzed for viability, apoptosis and necrosis. Representative flow cytometric scatter (A) and Annexin vs. PI plots (B) from cells treated with 20 µg/mL microparticles are shown. In (A), microspheres are distinguished from cells by their light scattering properties and are gated out of subsequent analysis. The average % viable cells (Annexin$^-$PI$^-$), apoptotic (Annexin$^+$PI$^-$/Annexin$^+$PI$^+$) and necrotic (Annexin$^-$PI$^+$) ± standard deviation of duplicate samples are plotted in C. There was no statistical difference in any population, as determined by t-test analysis, between untreated and treated samples, indicating that at these concentrations the microspheres are biologically compatible with Jurkat T-cells.

fluorescence intensity in the FA+ exposed cells as compared to the FA− exposed cells, indicating again that binding to the cell surface is mediated via the folic acid linker and is significantly stronger than non-specific adsorption.

3.7. Microsphere biocompatibility

To determine whether FFPDMS microspheres were biologically compatible with human cells, the leukemic T cell line, Jurkat, was incubated with various concentrations of small (1.7 ± 1.3 µm) microspheres for one day. Following exposure to microspheres the cells were labeled with fluorochrome (FITC)-conjugated Annexin V and the DNA binding dye, PI and analyzed for size and fluorescence by flow cytometry. Both microspheres and cells were detected by flow cytometry; microspheres were excluded from fluorescence analysis by gating based on light-scatter characteristics (Fig. 7A). Gated cells were then analyzed for PI and AnnexinV-FITC fluorescence. AnnexinV selectively binds to the membrane of cells undergoing apoptosis and PI enters and binds to the DNA of cells that have lost membrane integrity which occurs late in apoptosis or due to necrotic cell death. Therefore, dual fluorescence analysis allows for the discrimination between viable (Annexin$^-$PI$^-$), apoptotic (Annexin$^+$) and necrotic (Annexin$^-$PI$^+$) cells (Fig. 7B). Fig. 7C shows the distribution of each population in cells incubated without microspheres or with concentrations ranging from 0.2–20 µg/mL.

In a previous study, 10 µg/mL was shown to be an effective concentration for the delivery of chemotherapeutic agents by synthetic particles [64]. In addition, ~1 mg/mL has been suggested as a target value for magnetic nanoparticle concentration in targeted magnetic hyperthermia therapeutics [65], suggesting that nanoparticle concentrations in healthy tissues during treatment would be orders of magnitude lower. As shown in Fig. 7, there was no significant difference in survival

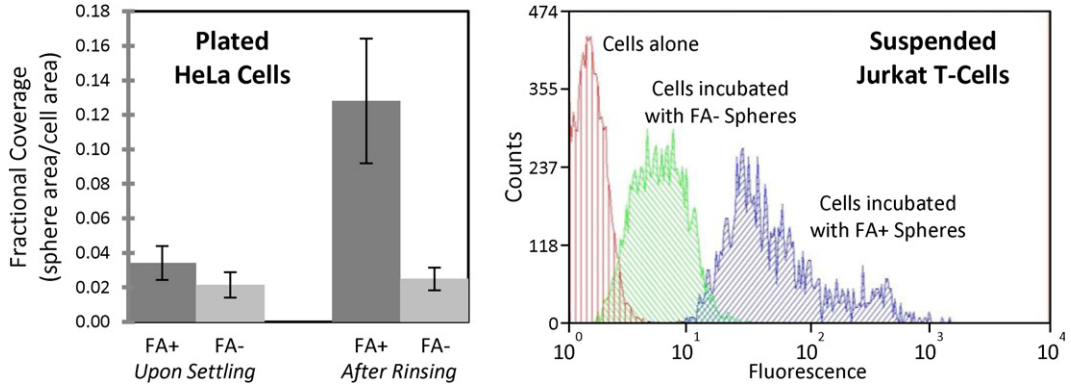

Fig. 6. Folate-functionalized FFPMDS microspheres preferentially bind to HeLa and Jurkat cells. Left: Alexa Fluor 488® conjugated FA+ and FA− spheres were incubated with adherent HeLa cells and the fraction of the total cell surface covered with spheres was measured by fluorescence microscopy both before and after rinsing. Turbulent flow during rinsing increases the incidence of contact between spheres and cell surfaces, resulting in markedly increased coverage by bound spheres in the FA+ condition. Right: The fluorescence intensity of Jurkat T cells alone or incubated with either AlexaFluor-488® conjugated FA− or FA+ spheres is shown.

or cell death due to exposure to average solution concentrations up to 20 μg/mL, suggesting that FFPDMS microspheres are biocompatible under these conditions. Even at concentrations as high as 200 μg/mL viability was only modestly reduced to 90% after one day and 83% after three days of exposure (data not shown). This concentration corresponds to approximately five microspheres per cell, which is more than sufficient for in vitro magnetic separation technologies such as magnetic-active cell sorting (MACS). Finally, it should be noted that all concentrations reported in this study refer to average values throughout the solution. However, rapid settling of both cells and microspheres during incubation results in dramatically increased local concentrations, which we conservatively estimate to be at least two orders of magnitude higher than reported values.

4. Conclusion

This work represents the first reported instance of silicone magnetic microspheres with diameters in the 2–50 μm size range. These spheres contain a high concentration of uniformly-distributed magnetic nanoparticles, lending them a magnetization which scales linearly with volume. We have demonstrated that these spheres provide an order-of-magnitude improvement in autofluorescence signal, which is vital to the sensitivity of fluorescence-based microsphere assays such as those used in IVD. We have also demonstrated an order-of-magnitude improvement in magnetic force generation compared to leading products in the 5–20 μm size range. By combining the non-contact advantages of magnetic microspheres with large forces generally achievable only by AFM, these microspheres introduce new possibilities in the fields of force spectroscopy and cellular mechanics.

In addition, we have shown that these silicone magnetic microspheres are biocompatible in concentrations relevant to potential in vivo and in vitro applications, and that they may be easily functionalized with a wide variety of ligands using existing and common chemical reactions. This enables their use in the full range of current magnetic microsphere applications with minimal to no modification of protocols.

Finally, the unique silicone matrix of our spheres suggests compatibility with several other applications. The matrix strongly absorbs organics, and therefore may be suitable for encapsulation and targeted delivery of poorly-soluble drugs such as taxanes, a common chemotherapeutic agent. The homogeneous, aggregate-free [47] dispersion of nanoparticles within the microspheres may be particularly well-suited for magnetic nanoparticle hyperthermia therapeutics, which suffers from the uncertainty of inter-particle interactions when un-encapsulated nanoparticles congregate in unknown concentrations at a targeted site. A microsphere formulation may provide rigorous control over local nanoparticle concentration while still maintaining a size-range compatible with targeted delivery and subsequent elimination (300–700 nm).

Acknowledgments

The authors wish to acknowledge Dr. Kris Ford of UNC Chapel Hill for providing the HeLa cells used in this study and for assisting us in their preparation, the Center for Computer Integrated Systems for Microscopy and Manipulation at UNC Chapel Hill for assistance with rheometry, and Nicholas Gomez, members of the Davis Lab, and the UNC Chapel Hill Lineberger Comprehensive Cancer Center for the use of their flow cytometry facilities. In addition, the authors gratefully acknowledge support from the Lumen Scholars program at Elon University, as well as continued support from the Elon University URP.

References

[1] D. Horak, M. Babic, H. Mackova, M.J. Benes, Preparation and properties of magnetic nano- and microsized particles for biological and environmental separations, J. Sep. Sci. 30 (2007) 1751–1772.
[2] F. Vartdal, G. Gaudernack, S. Funderud, A. Bratlie, T. Lea, J. Ugelstad, E. Thorsby, HLA class-I and class-II typing using cells positively selected from blood by immunomagnetic isolation — a fast and reliable technique, Tissue Antigens 28 (1986) 301–312.
[3] J.W. Choi, K.W. Oh, J.H. Thomas, W.R. Heineman, H.B. Halsall, J.H. Nevin, A.J. Helmicki, H.T. Henderson, C.H. Ahn, An integrated microfluidic biochemical detection system for protein analysis with magnetic bead-based sampling capabilities, Lab Chip 2 (2002) 27–30.
[4] T. Mitrelias, J. Palfreyman, Z. Jiang, J. Llandro, J.A.C. Bland, R.M. Sanchez-Martin, M. Bradley, Biological cell detection using ferromagnetic microbeads, J. Magn. Magn. Mater. 310 (2007) 2862–2864.
[5] J.C. He, M.Y. Huang, D.M. Wang, Z.M. Zhang, G.K. Li, Magnetic separation techniques in sample preparation for biological analysis: a review, J. Pharm. Biomed. Anal. 101 (2014) 84–101.
[6] M. Megens, M. Prins, Magnetic biochips: a new option for sensitive diagnostics, J. Magn. Magn. Mater. 293 (2005) 702–708.
[7] G. Kurlyandskaya, V. Levit, Advanced materials for drug delivery and biosensors based on magnetic label detection, Mater. Sci. Eng. C Biomim. Supramol. Syst. 27 (2007) 495–503.
[8] Y. Yang, Y. Morimoto, T. Takamura, A. Sandhu, Biosensing based on magnetically induced self-assembly of particles in magnetic colloids, J. Nanosci. Nanotechnol. 12 (2012) 2081–2088.
[9] W.C. Kuan, D. Horak, Z. Plichta, W.C. Lee, Immunocapture of CD133-positive cells from human cancer cell lines by using monodisperse magnetic poly(glycidyl methacrylate) microspheres containing amino groups, Mater. Sci. Eng. C Mater. Biol. Appl. 34 (2014) 193–200.
[10] J. Kucerova, Z. Svobodova, P. Knotek, J. Palarcik, M. Vlcek, M. Kincl, D. Horak, J. Autebert, J.L. Viovy, Z. Bilkova, PEGylation of magnetic poly(glycidyl methacrylate) microparticles for microfluidic bioassays, Mater. Sci. Eng. C Mater. Biol. Appl. 40 (2014) 308–315.
[11] A.R. Bausch, W. Moller, E. Sackmann, Measurement of local viscoelasticity and forces in living cells by magnetic tweezers, Biophys. J. 76 (1999) 573–579.
[12] M. Keller, J. Schilling, E. Sackmann, Oscillatory magnetic bead rheometer for complex fluid microrheometry, Rev. Sci. Instrum. 72 (2001) 3626–3634.
[13] J.A. Cribb, T.D. Meehan, S.M. Shah, K. Skinner, R. Superfine, Cylinders vs. spheres: biofluid shear thinning in driven nanoparticle transport, Ann. Biomed. Eng. 38 (2010) 3311–3322.
[14] R. Ajjan, B.C.B. Lim, K.F. Standeven, R. Harrand, S. Dolling, F. Phoenix, R. Greaves, R.H. Abou-Saleh, S. Connell, D.A.I. Smith, J.W. Weisel, P.J. Grant, R.A.S. Ariensl, Common variation in the C-terminal region of the fibrinogen beta-chain: effects on fibrin structure, fibrinolysis and clot rigidity, Blood 111 (2008) 643–650.
[15] C.T. Mierke, P. Kollmannsberger, D.P. Zitterbart, J. Smith, B. Fabry, W.H. Goldmann, Mechano-coupling and regulation of contractility by the vinculin tail domain, Biophys. J. 94 (2008) 661–670.
[16] G. Charvin, T.R. Strick, D. Bensimon, V. Croquette, Tracking topoisomerase activity at the single-molecule level, Annual Review of Biophysics and Biomolecular Structure, Annual Reviews, Palo Alto 2005, pp. 201–219.
[17] T.R. Strick, V. Croquette, D. Bensimon, Single-molecule analysis of DNA uncoiling by a type II topoisomerase, Nature 404 (2000) 901–904.
[18] A. Crut, D.A. Koster, R. Seidel, C.H. Wiggins, N.H. Dekker, Fast dynamics of supercoiled DNA revealed by single-molecule experiments, Proc. Natl. Acad. Sci. U. S. A. 104 (2007) 11957–11962.
[19] S. Selvam, D. Koirala, Z.B. Yu, H.B. Mao, Quantification of topological coupling between DNA superhelicity and G-quadruplex formation, J. Am. Chem. Soc. 136 (2014) 13967–13970.
[20] H.B. Peng, X.S.S. Ling, Reverse DNA translocation through a solid-state nanopore by magnetic tweezers, Nanotechnology 20 (2009) 8.
[21] V.S.K. Balagurusamy, P. Weinger, X.S. Ling, Detection of DNA hybridizations using solid-state nanopores, Nanotechnology 21 (2010) 9.
[22] N. Wang, J.P. Butler, D.E. Ingber, Mechanotransduction across the cell-surface and through the cytoskeleton, Science 260 (1993) 1124–1127.
[23] N. Bonakdar, A. Schilling, P. Lennert, M. Sporrer, R.C. Gerum, J.L. Alonso, W.H. Goldmann, Measuring mechanical properties in cells: three easy methods for biologists, Cell Biol. Int. 38 (2014) 1227–1232.
[24] A.R. Bausch, F. Ziemann, A.A. Boulbitch, K. Jacobson, E. Sackmann, Local measurements of viscoelastic parameters of adherent cell surfaces by magnetic bead microrheometry, Biophys. J. 75 (1998) 2038–2049.
[25] L. Chen, V. Maybeck, A. Offenhausser, H.J. Krause, Characterization of the mechanical properties of HL-1 cardiomyocytes with high throughput magnetic tweezers, Appl. Phys. Lett. 107 (2015) 4.
[26] J. Dobson, S.H. Cartmell, A. Keramane, A.J. El Haj, Principles and design of a novel magnetic force mechanical conditioning bioreactor for tissue engineering, stem cell conditioning, and dynamic in vitro screening, IEEE Trans. Nanobiosci. 5 (2006) 173–177.
[27] G.R. Kirkham, K.J. Elliot, A. Keramane, D.M. Salter, J.P. Dobson, A.J. El Haj, S.H. Cartmell, Hyperpolarization of human mesenchymal stem cells in response to magnetic force, IEEE Trans. Nanobiosci. 9 (2010) 71–74.
[28] F. Xu, R.G. Zhao, A.S. Liu, T. Metz, Y. Shi, P. Bose, D.H. Reich, A microfabricated magnetic actuation device for mechanical conditioning of arrays of 3D microtissues, Lab Chip 15 (2015) 2496–2503.
[29] I. Safarik, M. Safarikova, Use of magnetic techniques for the isolation of cells, J. Chromatogr. B 722 (1999) 33–53.
[30] M.S. Kim, G.H. Lee, J.M. Hong, H. Lee, Synthesis of monodisperse PS-co-PDMS microspheres by dispersion polymerization, Mater. Sci. Eng. C Biomim. Supramol. Syst. 27 (2007) 1247–1251.
[31] L. Gonzalez, B.G. Ma, L. Li, J.H. Hansen, S. Hvilsted, A.L. Skov, Encapsulated PDMS microspheres with reactive handles, Macromol. Mater. Eng. 299 (2014) 729–738.

[32] L. Gonzalez, M. Kostrzewska, B.G. Ma, L. Li, J.H. Hansen, S. Hvilsted, A.L. Skov, Preparation and characterization of silicone liquid core/polymer shell microcapsules via internal phase separation, Macromol. Mater. Eng. 299 (2014) 1259–1267.
[33] O. Dufaud, E. Favre, V. Sadtler, Porous elastomeric beads from crosslinked emulsions, J. Appl. Polym. Sci. 83 (2002) 967–971.
[34] G. Tepper, N. Levit, Polymer deposition from supercritical solutions for sensing applications, Ind. Eng. Chem. Res. 39 (2000) 4445–4449.
[35] Q. Tang, J.R. Yu, L. Chen, J. Zhu, Z.M. Hu, Porous silicone hydrogel interpenetrating polymer networks prepared using a template method for biomedical use, Polym. Int. 60 (2011) 1136–1141.
[36] P.K. Roy, N. Iqbal, D. Kumar, C. Rajagopal, Polysiloxane-based core–shell microspheres for toughening of epoxy resins, J. Polym. Res. 21 (2014) 9.
[37] J.M. Rankin, N.K. Neelakanta, K.E. Lundberg, E.M. Grzincic, C.J. Murphy, K.S. Suslick, Magnetic, fluorescent, and copolymeric silicone microspheres, Adv. Sci. 2 (2015).
[38] S.L. Peng, M.Y. Zhang, X.Z. Niu, W.J. Wen, P. Sheng, Z.Y. Liu, J. Shi, Magnetically responsive elastic microspheres, Appl. Phys. Lett. 92 (2008) 3.
[39] B.L. Zhang, H.P. Zhang, X.J. Li, X.F. Lei, C.M. Li, D.Z. Yin, X.L. Fan, Q.Y. Zhang, Synthesis of BSA/Fe_3O_4 magnetic composite microspheres for adsorption of antibiotics, Mater. Sci. Eng. C Mater. Biol. Appl. 33 (2013) 4401–4408.
[40] F.G. Guo, Q.Y. Zhang, W.W. Wang, H.P. Zhang, J.L. Sun, Preparation of pH-responsive Fe_3O_4/poly (acrylic acid-stat-methyl methacrylate-block-(2-dimethylamino) ethyl methacrylate) magnetic composite microspheres and its application in controlled release of drug, Mater. Sci. Eng. C Mater. Biol. Appl. 31 (2011) 938–944.
[41] A. Chandna, D. Batra, S. Kakar, R. Singh, A review on target drug delivery: magnetic microspheres, J. Acute Dis. (2013) 189–195.
[42] L.H. Azouz, F. Dahmoune, F. Rezgui, C. G'Sell, Full factorial design optimization of anti-inflammatory drug release by PCL–PEG–PCL microspheres, Mater. Sci. Eng. C Mater. Biol. Appl. 58 (2016) 412–419.
[43] C. Berkland, M.J. Kipper, B. Narasimhan, K.K. Kim, D.W. Pack, Microsphere size, precipitation kinetics and drug distribution control drug release from biodegradable polyanhydride microspheres, J. Control. Release 94 (2004) 129–141.
[44] B. Luo, S.A. Xu, A. Luo, W.R. Wang, S.L. Wang, J. Guo, Y. Lin, D.Y. Zhao, C.C. Wang, Mesoporous biocompatible and acid-degradable magnetic colloidal nanocrystal clusters with sustainable stability and high hydrophobic drug loading capacity, ACS Nano 5 (2011) 1428–1435.
[45] C. Liu, J. Guo, W. Yang, J. Hu, C. Wang, S. Fu, Magnetic mesoporous silica microspheres with thermo-sensitive polymer shell for controlled drug release, J. Mater. Chem. 19 (2009) 4764–4770.
[46] A.H. Najafabadi, M. Abdouss, S. Faghihi, Synthesis and evaluation of PEG-O-chitosan nanoparticles for delivery of poor water soluble drugs: ibuprofen, Mater. Sci. Eng. C Mater. Biol. Appl. 41 (2014) 91–99.
[47] B.A. Evans, B.L. Fiser, W.J. Prins, D.J. Rapp, A.R. Shields, D.R. Glass, R. Superfine, A highly tunable silicone-based magnetic elastomer with nanoscale homogeneity, J. Magn. Magn. Mater. 324 (2012).
[48] R. Massart, Preparation of aqueous magnetic liquids in alkaline and acidic media, IEEE Trans. Magn. 17 (1981) 1247–1248.
[49] M. Zborowski, L.R. Moore, P.S. Williams, J.J. Chalmers, Separations based on magnetophoretic mobility, Sep. Sci. Technol. 37 (2002) 3611–3633.
[50] N. Pamme, J.C.T. Eijkel, A. Manz, On-chip free-flow magnetophoresis: separation and detection of mixtures of magnetic particles in continuous flow, J. Magn. Magn. Mater. 307 (2006) 237–244.
[51] D. Cheng, K. Halvorsen, W.P. Wong, Note: high-precision microsphere sorting using velocity sedimentation, Rev. Sci. Instrum. 81 (2010) 3.
[52] S. Dutz, J.H. Clement, D. Eberbeck, T. Gelbrich, R. Hergt, R. Mueller, J. Wotschadlo, M. Zeisberger, Ferrofluids of magnetic multicore nanoparticles for biomedical applications, J. Magn. Magn. Mater. 321 (2009) 1501–1504.
[53] N. Pamme, Continuous flow separations in microfluidic devices, Lab Chip 7 (2007) 1644–1659.
[54] J.C. Giddings, Field-flow fractionation — analysis of macromolecular, colloidal, and particulate materials, Science 260 (1993) 1456–1465.
[55] M. Yamada, M. Nakashima, M. Seki, Pinched flow fractionation: continuous size separation of particles utilizing a laminar flow profile in a pinched microchannel, Anal. Chem. 76 (2004) 5465–5471.
[56] C. Gosse, V. Croquette, Magnetic tweezers: micromanipulation and force measurement at the molecular level, Biophys. J. 82 (2002) 3314–3329.
[57] J. Lipfert, X.M. Hao, N.H. Dekker, Quantitative modeling and optimization of magnetic tweezers, Biophys. J. 96 (2009) 5040–5049.
[58] K.C. Neuman, A. Nagy, Single-molecule force spectroscopy: optical tweezers, magnetic tweezers and atomic force microscopy, Nat. Methods 5 (2008) 491–505.
[59] C. Sun, R. Sze, M.Q. Zhang, Folic acid-PEG conjugated superparamagnetic nanoparticles for targeted cellular uptake and detection by MRI, J. Biomed. Mater. Res. A 78A (2006) 550–557.
[60] S. Mohapatra, S.K. Mallick, T.K. Maiti, S.K. Ghosh, P. Pramanik, Synthesis of highly stable folic acid conjugated magnetite nanoparticles for targeting cancer cells, Nanotechnology 18 (2007).
[61] P.S. Low, S.A. Kularatne, Folate-targeted therapeutic and imaging agents for cancer, Curr. Opin. Chem. Biol. 13 (2009) 256–262.
[62] D. Yang, K. Wei, Q. Liu, Y. Yang, X. Guo, H. Rong, M.-L. Cheng, G. Wang, Folic acid-functionalized magnetic $ZnFe_2O_4$ hollow microsphere core/mesoporous silica shell composite particles: synthesis and application in drug release, Mater. Sci. Eng. C Mater. Biol. Appl. 33 (2013) 2879–2884.
[63] N. Ngernyuang, W. Seubwai, S. Daduang, P. Boonsiri, T. Limpaiboon, J. Daduang, Targeted delivery of 5-fluorouracil to cholangiocarcinoma cells using folic acid as a targeting agent, Mater. Sci. Eng. C Mater. Biol. Appl. 60 (2016) 411–415.
[64] H. Unterweger, R. Tietze, C. Janko, J. Zaloga, S. Lyer, S. Durr, N. Taccardi, O.M. Goudouri, A. Hoppe, D. Eberbeck, D.W. Schubert, A.R. Boccaccini, C. Alexiou, Development and characterization of magnetic iron oxide nanoparticles with a cisplatin-bearing polymer coating for targeted drug delivery, Int. J. Nanomedicine 9 (2014) 3659–3676.
[65] H. Mamiya, Recent advances in understanding magnetic nanoparticles in AC magnetic fields and optimal design for targeted hyperthermia, J. Nanomater. 17 (2013).